Case Studies in Nondestructive Testing and Evaluation 5 (2016) 9–14

Contents lists available at ScienceDirect

Case Studies in Nondestructive Testing and Evaluation

www.elsevier.com/locate/csndt

Fabrication of imitative cracks by 3D printing for electromagnetic nondestructive testing and evaluations

Noritaka Yusa *, Weixi Chen, Jing Wang, Hidetoshi Hashizume

Department of Quantum Science and Energy Engineering, Graduate School of Engineering, Tohoku University, 6-6-01-2, Aramaki Aza Aoba, Aoba-ku, Sendai, Miyagi 980-8579, Japan

ARTICLE INFO

Article history:
Available online 31 March 2016

ABSTRACT

This study demonstrates that 3D printing technology offers a simple, easy, and cost-effective method to fabricate artificial flaws simulating real cracks from the viewpoint of eddy current testing. The method does not attempt to produce a flaw whose morphology mirrors that of a real crack but instead produces a relatively simple artificial flaw. The parameters of this flaw that have dominant effects on eddy current signals can be quantitatively controlled. Three artificial flaws in type 316L austenitic stainless steel plates were fabricated using a powderbed-based laser metal additive manufacturing machine. The three artificial flaws were designed to have the same length, depth, and opening but different branching and electrical contacts between flaw surfaces. The flaws were measured by eddy current testing using an absolute type pancake probe. The signals due to the three flaws clearly differed from each other although the flaws had the same length and depth. These results were supported by subsequent destructive tests and finite element analyses.

1. Introduction

Surface breaking cracks are among the most harmful degradations of structures. In general in-service inspections, visual, penetrant, or magnetic particle tests are conducted to detect surface breaking cracks, and if a crack is detected subsequent ultrasonic tests are performed to size the crack to determine suitable action. Eddy current testing (ECT) has drawn attention because recent studies have demonstrated that ECT can both detect and quantitatively evaluate cracks [1,2]. However, most studies to date have used artificial slits to simulate cracks even though the signals caused by an artificial slit can sometimes differ significantly from those caused by a real crack. Because the availability of real cracks is quite limited, techniques to produce artificial flaws that simulate real cracks are indispensable for further studies regarding the application of ECT to enhance structure maintenance.

Techniques to efficiently create thermal fatigue cracks [3] and stress corrosion cracks [4,5] for nondestructive tests have been proposed, and these methods produce cracks with very similar morphology to actual cracks. However, qualitative discussion of morphology is not always sufficient from the viewpoint of non-destructive signals. It is more reasonable to focus on specific factors that have dominant effects on nondestructive signals. In addition, because the length and depth of a flaw must be known to evaluate its effect on structural integrity, both of these factors should be accurately controlled so the sample need not be destroyed to confirm them. Fine processing technology including focused ion beam and sputtering

* Corresponding author. Tel.: +81 (0)22 795 6319; fax: +81 (0)22 795 6319.
E-mail address: noritaka.yusa@qse.tohoku.ac.jp (N. Yusa).

http://dx.doi.org/10.1016/j.csndt.2016.03.004

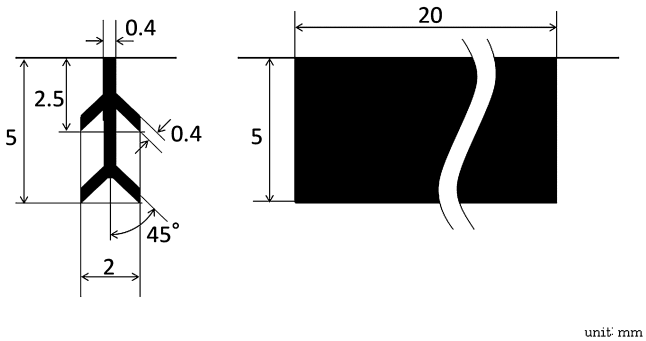

Fig. 1. Profile of Flaw B.

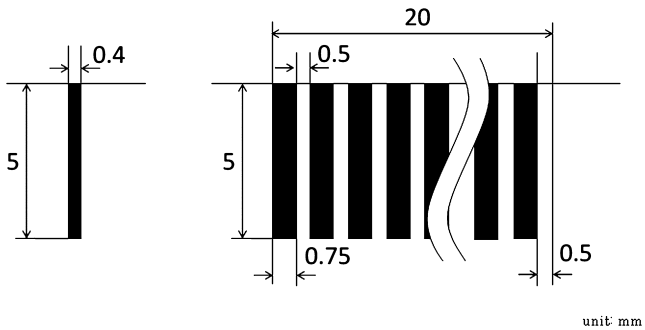

Fig. 2. Profile of Flaw C.

could enable to reproduce three-dimensional structure of actual cracks; however it is not realistic to fabricate samples and flaws sufficiently large for the purpose of general nondestructive testing.

To address this issue, earlier studies have proposed embedding an artificial discontinuity inside a material using diffusion bonding to simulate a real crack from the viewpoint of ECT [6,7]. Because ECT is relatively insensitive to flaw microstructure, a crack can be regarded as a region with a simple geometry and nearly uniform electromagnetic characteristics different from those of the base metal. Therefore embedding an artificial discontinuity with a structure finer than the spatial resolution of ECT could simulate a real crack. Although this method would be simple and cost-effective, significant preliminary testing is required to find suitable bonding conditions which depend on the strength of the material. Additionally, the unidirectional stress necessary for bonding restricts the sample shape and the three-dimensional flaw structure.

Based on the above background, this study proposes another approach, the application of 3D printing technology, to easily prepare artificial flaws simulating real cracks. Several artificial flaws embedded in type 316L austenitic stainless steel plates were fabricated. Eddy current and subsequent destructive tests were conducted. The results of the tests were analyzed using three-dimensional finite element simulations, demonstrating the validity of the approach.

2. Materials and methods

2.1. Fabricating artificial flaws using 3D printing technology

Whereas the length and depth of a crack have dominant effects on non-destructive signals, other factors affecting the signals strongly depend on the non-destructive testing method applied [8]. For example, crack closure, which significantly affects the signals of ultrasonic tests [9], has little effect on eddy current signals [10–12]. A recent study has evaluated the effect of the oxide layer on ECT signals [13], whose results point out the difficult of quantitatively controlling the degree of eddy currents across a flaw by artificially introducing the oxide layer. More macroscopic characteristics, such as crack branching [14] and the degree of eddy currents across a flaw [15–18], affect eddy current signals and their analysis for flaw evaluation.

On the basis of this, this study fabricated three flaws, which are hereafter denoted as Flaws A, B and C. Flaw A is a simple rectangular slit with a surface length of 20 mm, depth of 5 mm, and opening of 0.4 mm, which was fabricated as a reference. Flaw B illustrated in Fig. 1 simulates a flaw branched inside a material, which is difficult to fabricate using conventional machining. Flaw C illustrated in Fig. 2 consists of 16 equally spaced columns, which simulates a flaw across which part of the induced eddy currents flows. All of the flaws were designed to have the same surface length, maximum depth, and crack opening. The flaws were introduced into a type 316L austenitic stainless steel plate with a thickness of 7 mm and dimensions of approximately 70 mm $\times$ 45 mm.

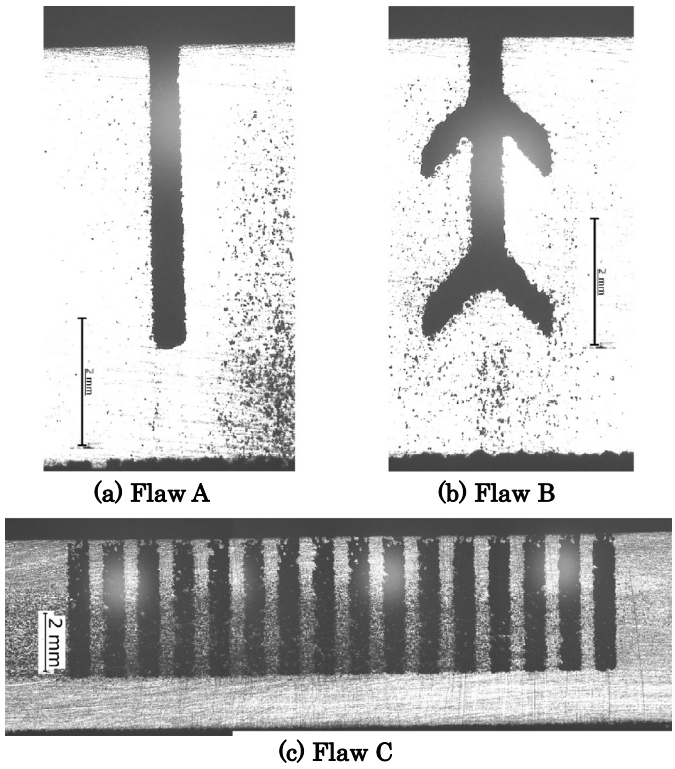

Fig. 3. Cross-sectional profiles of the flaws. The three flaws had a depth of 4.9 mm.

The samples containing the flaws were fabricated using a powderbed-based laser metal additive manufacturing machine, M2 cusing (Concept Laser GMBH, Lichtenfels, Germany). Type 316L austenitic stainless steel powder particles with a diameter of 25–30 μm were paved on a powder bed and melted using a laser with an intensity of 200 W to form a thin cross section of the sample. The thickness of the layer was 30 μm, which was sufficiently below the spatial resolution of typical ECT. The surfaces of the samples were polished using a waterproof abrasive paper after this additive manufacturing process to a roughness of approximately Ra = 0.04 μm (JIS2001), which reasonably simulated the surface of a general structure made of type 316L austenitic stainless steel.

2.2. Evaluation of the fabricated artificial flaws

2.2.1. Eddy current examination

Eddy current examinations were conducted using a commercial eddy current instrument, aect2000N (Aswan ECT Co., Ltd., Osaka, Japan), and an absolute type pancake probe with a height, inner diameter, and outer diameter of 0.8, 1.2, and 3.2 mm, respectively. An exciting frequency of 25 kHz was adopted; the probe scanned across the flaw to gather eddy current signals. A thick plastic plate was attached at the surface of the sample, and the scanning was conducted manually while pressing the probe against the board to realize a constant lift-off of 0.2 mm.

2.2.2. Visual examination

After the eddy current examination, the samples were destroyed to confirm the cross-sectional profiles of the flaws. Based on the flaw profiles, Flaws A and B were observed on a plane perpendicular to the flaw, and Flaw C was observed on a plane parallel to the flaw.

2.2.3. Finite element analysis

Finite element simulations using the commercial software, Comsol Multiphysics version 5.1 and its AC/DC module, were conducted to validate the measured eddy current signals. The simulations were performed in the frequency domain with the magnetic vector potential formulation. Flaws A and B were precisely modeled in the simulations. In contrast, two models were used to simulate the signals due to Flaw C. The first, Model 1, modeled Flaw C as illustrated in Fig. 2; the other, Model 2, modeled Flaw C as a rectangular region with a length of 20 mm, depth of 5 mm, constant width of 0.4 mm, and uniform conductivity inside. The conductivity and relative permeability of the base metal were set to 1.35 MS/m and 1, respectively.

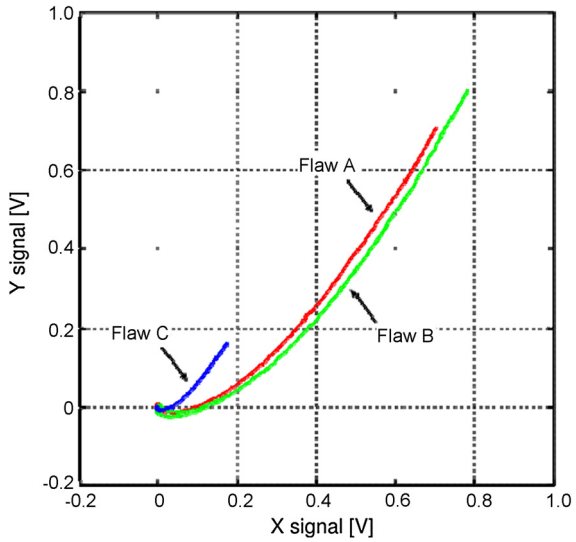

Fig. 4. Eddy current signals due to the artificial flaws.

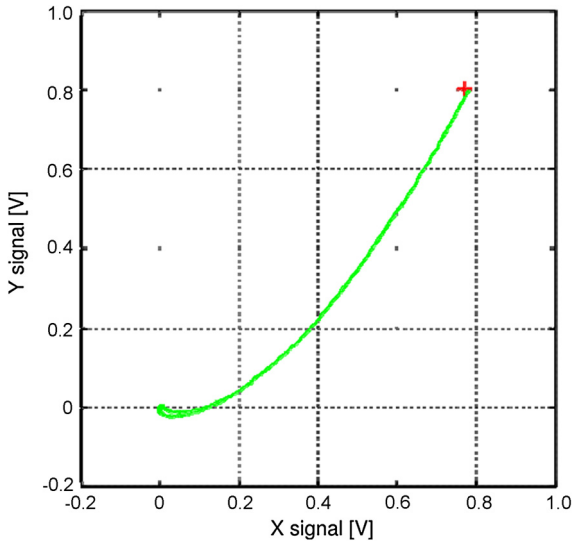

Fig. 5. Comparison between measured (lines) and simulated (marks) signals of Flaw B.

3. Results and discussion

Fig. 3 shows the results of the visual examinations. The figure confirms that on the whole the actual profiles of the flaws agree with the designed ones. Closer observation reveals that Flaw A had an opening of 0.48–0.53 mm, which is approximately 0.1 mm wider than the design, and a depth of 4.9 mm, which is 0.1 mm shallower than the design. The bottom of the flaw is not flat but somewhat curved. These imply that the accuracy of fabricating flaws is limited to a few hundred micro millimeters, which can be regarded as sufficiently fine comparing with the spatial resolution of typical ECT. In addition, small voids observed on the right–bottom of the picture reveals that the powders were not completely melted. These characteristics are more conspicuous on the actual profile of Flaws B and C; the presence of voids on the cross-sectional profile of Flaw C implies that the electrical resistance of the flaw was larger than the designed one.

The measured eddy current signals are shown in Fig. 4. The signals are calibrated so that the maximum signal caused by Flaw A has an amplitude of 1 V and a phase of 45 degree. Although the three flaws had the same length and depth, clear differences existed between their signals. Branching increased eddy current signals, while the presence of eddy currents flowing across a crack decreased eddy current signals; these results are consistent to those of earlier numerical simulation studies [14,17].

The results of the finite element simulations are summarized in Figs. 5 and 6. The simulated signals are also calibrated so that the maximum signal due to Flaw A has an amplitude of 1 V and a phase of 45 degree, which enables to compare

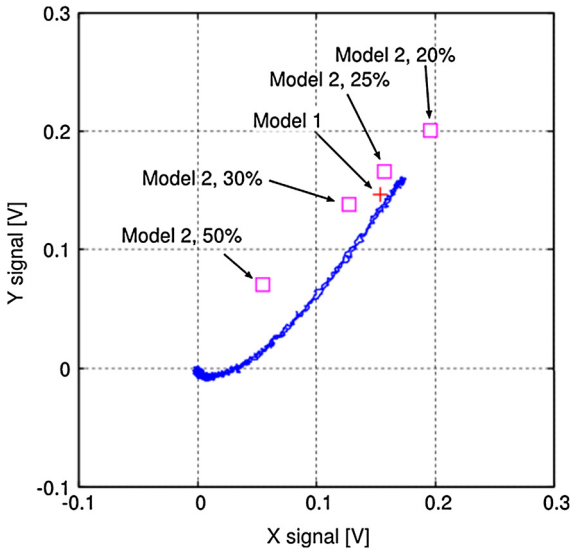

Fig. 6. Comparison between measured (lines) and simulated (marks) signals of Flaw C. Digits shown after 'Model 2' indicate the electrical conductivity of a flaw in a percentage of base material's conductivity.

them directly with the measured signals. The good agreement in the signals shown in Fig. 5 confirms little effects of the presence of the voids and the slight difference between the designed and actual profiles of the flaw. This supports the effectiveness of 3D printing technology to fabricate a flaw with branching. Fig. 6 shows that the signal obtained by the numerical simulation using Model 1, which modeled Flaw C accurately, is almost 10% smaller than measured ones. Whereas the presence of the voids would support this, the complexity of the profile of Flaw C implies that this difference would be acceptable because simulated and precisely measured eddy current signals have a difference of several percent even when they are due to a simple rectangular slit [19,20]. Numerical simulations using Model 2 revealed that assuming a uniform conductivity of approximately 25% of base material's one provides good agreement between the simulated and measured signals. Recent studies have revealed that in most cases modeling a flaw as a simple rectangular or semielliptic region with uniform internal conductivity reasonably simulates eddy current signals due to the flaw, even when part of the induced eddy currents flows across the flaw [17,18]. These results support the validity of Flaw C as a simulation of real cracks that do not behave as insulating walls.

4. Conclusion

This study has proposed the fabrication of artificial flaws simulating that simulate real cracks from the viewpoint of ECT using 3D printing technology. Three artificial flaws in type 316L austenitic stainless steel plates were fabricated to demonstrate that it is possible to quantitatively control not only the length and depth of a flaw, but also its branching and electrical resistance, all which significantly affect its eddy current signals. The validity of the proposed approach was confirmed by eddy current examination, visual examination, and finite element analysis. The densities of the samples fabricated in this study were 7.7 g/cm^3, which is approximately 96% of the density of general 316L austenitic stainless steel. No obvious attractive force was confirmed between the samples and permanent magnets, which supports to regard the samples as nonmagnetic. These, as well as the good agreement between the experiment and the simulations, indicate that it is reasonable to regard the samples are basically identical to general type 316L austenitic steel.

It should be noted that all information concerning flaw fabrication is recorded in an STL file that can be prepared using CAD software, and no special techniques are necessary. This enables very accurately controllable cracks to be fabricated with high reproductivity. It should be also noted that the machine and raw materials used in this study were generic; no special fabrication instruments were necessary. Although sample fabrication for the present study required over 10 hours, recent developments in 3D printing technology suggest that, in the future, it will be possible to fabricate artificial flaws simulating real cracks with greatly reduced time and cost. It will also be possible to fabricate artificial flaws for other nondestructive testing methods, such as ultrasonic tests, that are more sensitive to microscopic flaw structure.

Acknowledgements

This work was partially supported by JSPS KAKENHI Number 26220913.

References

[1] Bowler JR. Review of eddy current inversion with application to nondestructive evaluation. Int J Appl Electromagn Mech 1997;8:3–16.

[2] Auld BA, Moulder JC. Review of advances in quantitative eddy current nondestructive evaluation. J Nondestruct Eval 1999;18:3–36.
[3] Kemppainen M, Virkkunen I, Pitkänen J, Paussu R, Hänninen H. Advanced flaw production method for in-service inspection qualification mock-ups. J Nucl Eng Des 2003;224:105–17.
[4] Bahn CB, Bakhtiari S, Park J, Majumdar S. Manufacturing of representative axial stress corrosion cracks in tube specimens for eddy current testing. Nucl Eng Des 2013;256:38–44.
[5] Lee TH, Hwang IS, Kim HD, Kim JH. Techniques for intergranular crack formation and assessment in alloy 600 base and alloy 182 metals. Nucl Eng Technol 2015;47:102–14.
[6] Yusa N, Uchimoto T, Takagi T, Hashizume H. An accurately controllable imitative stress corrosion cracking for electromagnetic nondestructive testing and evaluation. Nucl Eng Des 2012;245:1–7.
[7] Yusa N, Hashizume H. Fabrication of imitative stress corrosion cracking specimen using lithography and solid state bonding. Int J Appl Electromagn Mech 2012;39:291–6.
[8] Clark R, Dover WD, Bond LJ. The effect of crack closure on the reliability of NDT predictions of crack size. NDT Int 1987;20:269–75.
[9] Ohara Y, Shintaku Y, Horinouchi S, Ikeuchi M, Yamanaka K. Enhancement of selectivity in nonlinear ultrasonic imaging of closed cracks using amplitude difference phased array. Jpn J Appl Phys 2012;51:07GB18.
[10] Yusa N, Perrin S, Mizuno K, Chen Z, Miya K. Eddy current inspection of closed fatigue and stress corrosion cracks. Meas Sci Technol 2007;18:3403–8.
[11] Kurokawa M, Kamimura T, Fukui S. Relationship between electric properties and width of cracks of Inconel alloy. In: Proceedings of the 13th international conference on NDE in the nuclear and pressure vessel industries. 1995. p. 261–5.
[12] Chen Z, Yusa N, Miya K, Tokuma H. Effect of crack closure on quantitative ECT inspection of closed fatigue cracks. In: Tamburrino A, Melikhov Y, Chen Z, Udpa L, editors. Electromagnetic nondestructive evaluation (XI). IOS Press; 2008. p. 171–8.
[13] Uchimoto T, Takagi T, Ohtaki K, Takeda Y, Kawakami A. Electromagnetic modeling of fatigue cracks in plant environment for eddy current testing. Int J Appl Electromagn Mech 2012;39:261–8.
[14] Cheng W, Kanemoto S, Komura I. Numerical evaluation of the depth of branched-off cracks using eddy current testing. IEEE Trans Magn 2008;44:1030–3.
[15] Villone F, Harfield N. Simulation of the effects of current leakage across thin cracks. In: Udpa SS, Takagi T, Pavo J, Albanese R, editors. Electromagnetic nondestructive evaluation (IV). IOS Press; 1999. p. 79–86.
[16] Yusa N, Chen Z, Miya K, Uchimoto T, Takagi T. Large-scale parallel computation for the reconstruction of natural stress corrosion cracks from eddy current testing signals. NDT E Int 2003;36:449–59.
[17] Yusa N, Perrin S, Mizuno K, Miya K. Numerical modeling of general cracks from the viewpoint of eddy current testing. NDT E Int 2007;40:577–83.
[18] Yusa N, Hashizume H. Evaluation of stress corrosion cracking as a function of its resistance to eddy currents. Nucl Eng Des 2009;239:2713–8.
[19] Takagi T, Fukutomi H. Benchmark activities of eddy current testing for steam generator tubes. In: Udpa SS, et al., editors. Electromagnetic nondestructive evaluation (IV). IOS Press; 2000. p. 235–52.
[20] Yusa N, Hashizume H. Numerical investigation of the ability of eddy current testing to size surface breaking cracks. Nondestruct Test Eval 2016. http://dx.doi.org/10.1080/10589759.2015.1135918.